

# Efficient Hydrothermal Synthesis of Flake-Like Molybdenum Disulfide for Selective Electrochemical Detection of Metol in Water Real Samples

Chelliah Kovenathan<sup>1</sup>, Venkatachalam Vinothkumar<sup>1</sup>, Shen-Ming Chen<sup>1,\*</sup>, Tse-Wei Chen<sup>1,2</sup>, Arumugam Sangili<sup>1</sup>, Karuppiyah Pandi<sup>1</sup>, and Venkatachalam Sethupathi<sup>1</sup>

<sup>1</sup> Department of Chemical Engineering and Biotechnology, National Taipei University of Technology, No. 1, Chung-Hsiao East Road, Section 3, Taipei 10608, Taiwan.

<sup>2</sup> Research and Development Center for Smart Textile Technology, National Taipei University of Technology, Taiwan

\*E-mail: [smchen78@ms15.hinet.net](mailto:smchen78@ms15.hinet.net)

Received: 2 April 2020 / Accepted: 30 May 2020 / Published: 10 July 2020

---

Transition metal chalcogenide has great interest owing to unique structural properties, higher conductivity, larger electroactive surface area, and excellent catalytic response. Herein, we have synthesized flake like MoS<sub>2</sub> via the simple hydrothermal method for electrochemical detection of Metol (MT). For spectral analysis, X-ray diffraction, Fourier transform infrared instrument, Field Emission Electron Microscopy, and elemental mapping displays successfully formation of flake-like MoS<sub>2</sub>. The electrochemical activity was tested in electrochemical impedance spectroscopy, cyclic voltammetry, differential pulse voltammetric techniques. As a result, the proposed sensor shows the excellent active surface area is 0.78 cm<sup>2</sup>, lower peak to peak separation is 0.24 V, respectively. Moreover, the flake-like electrode exhibits a wide linear range from 0.2 to 1211 μM, the low detection limit is 0.01 μM, with the higher sensitivity is 1.05 μA μM<sup>-1</sup> cm<sup>-2</sup> in the detection of MT. Furthermore, MoS<sub>2</sub> modified SPCE demonstrates enrich selectivity, stability, reproducibility, repeatability during the detection of MT. Finally, the real-time application was applied in river and tap water samples with acceptable recoveries of MT detection.

---

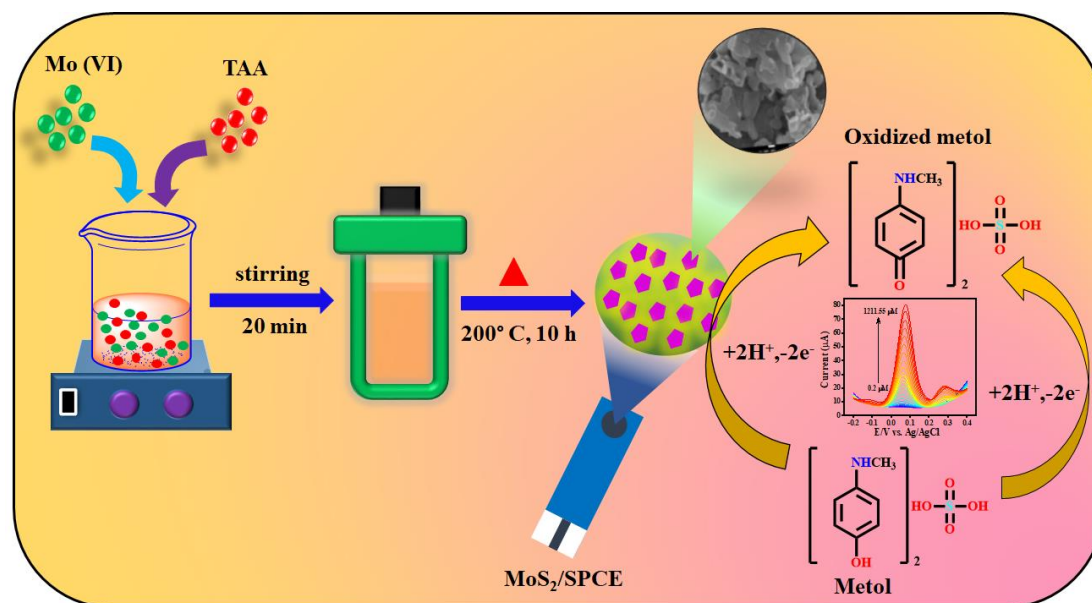
**Keywords:** Molybdenum disulfide, flake-like nanostructure, metol, electrochemical sensor, water samples.

## 1. INTRODUCTION

Metol (MT, N-Methyl-p-aminophenol sulfate) is an organic compound contains amine (–NH<sub>2</sub>) and hydroxyl groups (–OH) [1], which is one of the monochromic chemical used as a photographic development and hair dye. In the cause of metol shows toxicity, environmental, water, and industrial

wastewater pollution [2]. However, it will take a high level of MT to affect a lot of health problems such as eye irritation, slower heartbeat, skin allergy, damage to internal sources in the human body. Therefore, we need to develop a simple, rapid, cost-effective, and higher sensitivity of MT detection. So far, various analytical techniques determined in MT including spectrophotometry [3], Fenton reagent [4], ceric oxidimetry [5], photolysis [6], chromatogram mass-spectrometry [7], and oscillopolarographic titration [8]. Based on these methods are higher cost, complicated process, difficult to handle, and time variation. On the other hand, electrochemical is one of the most efficient techniques for real-time monitoring, rapid analysis, cost-effectiveness, fast response, and high sensitivity.

Nowadays, nanomaterials have great attention because of their unique structural and electrical properties. In particular, 2D transition metal chalcogenide such as  $\text{MX}_2$  (where  $\text{M} = \text{Mo}, \text{W}, \text{V}, \text{Ta}, \text{Ti}, \text{Zr}, \text{Sb}; \text{X} = \text{S}, \text{Se}, \text{Te}$ ) have been impressive research due to their enormous optical, physicochemical properties, and better conductivity in the fields of photocatalysis [9], capacitors [10], batteries [11], fuel cells [12], hydrogen evolution reaction [13], oxygen reduction reaction [14], and electrochemical sensors [15]. Among them, molybdenum disulfide ( $\text{MoS}_2$ ) was known to be an significant 2D nanomaterial for electrochemical applications because of their its highly exposed active sides, higher ionic conductivity compared to the oxides, high electron mobility, and layered depended band gap [16]. The nanostructure of molybdenum disulfide ( $\text{MoS}_2$ ) prepared for various methods such as thermal exfoliation process [17], solvothermal method [18], gas-phase synthesis [19], and chemical vapor deposition [20]. Compare to these, the hydrothermal technique shows well-shown shapes, larger charge transfer capability, excellent porosity, and superior electrocatalytic activity. Therefore, very few reports only available to the detection of MT. To the best of our knowledge, there is no reported in the flake-like  $\text{MoS}_2$  modified electrode for the MT detection with lower LOD.



**Scheme 1.** Schematic diagram of the synthesis of flake-like  $\text{MoS}_2$  and their electrocatalytic performance of metol.

In this work, we have demonstrated flake like MoS<sub>2</sub> via a simple hydrothermal method during the electrochemical determination of MT (Scheme 1). Further, the prepared modified electrode was applied for various spectroscopic techniques, including XRD, FTIR, and FESEM with mapping analysis. The electrocatalytic activity of MoS<sub>2</sub> modified SPCE displays a lower charge transfer coefficient, highest redox peak current, and larger active surface area. It is suggesting that MoS<sub>2</sub>/SPCE has superior catalytic performance in the metal detection. Furthermore, the fabricated sensor shows a wide linear response, lower detection limit with better sensitivity and satisfactory recoveries of various water samples of MT.

## 2. EXPERIMENTAL

### 2.1 Chemicals and reagents

Sodium molybdate dihydrate (Na<sub>2</sub>MoO<sub>4</sub>·2H<sub>2</sub>O, ≥ 99.5%), thioacetamide (TAA) (C<sub>2</sub>H<sub>5</sub>NS, ≥ 99.0%), metal (4-(methylamino) phenol hemisulfate) (C<sub>7</sub>H<sub>9</sub>NO·0.5HSO<sub>4</sub>, ≥ 98.0%), were purchased from Sigma Aldrich. For electrochemical analysis, the supporting electrolyte solution was made by monosodium hydrogen phosphate (Na<sub>2</sub>HPO<sub>4</sub>, 99%) and disodium hydrogen phosphate (NaH<sub>2</sub>PO<sub>4</sub>, 98%) and the pH buffer solution were adjusted by adding of NaOH & concentrated HCl. All experiments were used for Millipore water (18.2 M W/cm, Milli-Q).

### 2.2 Characterization methods

The purity of the sample was analyzed by X-ray diffraction (XRD) using performed PANalytical X'PERT PRO diffractometer (Cu K $\alpha$  radiation ( $\lambda$ = 1.5417 Å)). The presence of functional groups as synthesis MoS<sub>2</sub> was characterized using Fourier transform infrared instrument (FTIR) (FTIR-6600 spectrometer) in the transmission of the wavenumber. The morphology of the samples was characterized by field emission scanning electron microscopy (FESEM, JEOLJSM-6500F). Finally, energy dispersive X-ray spectroscopic (EDX) with elemental mapping were analyzed from the synthesized material.

### 2.3 Electrochemical analysis

Electrochemical impedance spectroscopy (EIS) was performed in the frequency range of 10<sup>-2</sup>–10<sup>5</sup> Hz (EIS, IM6ex ZAHNER impedance measurement unit). Electrochemical studies of nanoflake like MoS<sub>2</sub> were examined by cyclic voltammetry (CV) and differential pulse voltammetry (DPV) using CHI900 and CHI1205b electrochemical analyzer. Further, all the measurements were analyzed for the conventional three-electrode system with platinum (Pt) wire as the counter electrode, screen-printed carbon electrode (SPCE) is a working electrode, saturated Ag/AgCl used for reference electrode and platinum wire as the counter electrode. In addition, CV and DPV measurements were applied in the potential of -0.2 to 0.4 V (vs. Ag/AgCl) using 0.05 M PBS solution.

#### 2.4 Synthesis of flake-like MoS<sub>2</sub>

Nanostructure based flake like MoS<sub>2</sub> was synthesized by one-step hydrothermal method using molybdenum and sulfur sources, respectively. In this process, 0.5 M of Sodium molybdate dehydrate and 2.5 M of thioacetamide was dissolved in 60 mL of distilled water with continuous stirring for 0.5 h. The above homogeneous solution was mixed then transferred into a 100-mL Teflon-lined autoclave and heated at 200 °C for 10 h. After the reaction cooled down naturally, the obtained product was washed with distilled water and ethanol several times. Further, the samples were drying in a hot air oven at 60 °C for 12 h. Finally, the collected powder was used for further characterizations and electrochemical measurements.

#### 2.5 Fabrication of MoS<sub>2</sub> modified SPCE

Flake like MoS<sub>2</sub> (5.0 mg) was dispersed in 1.0 mL of Millipore water followed by ultrasonication for 15 min. Then, 8.0 µL of MoS<sub>2</sub> material was drop cast on SPCE and dried at 50°C for 15 min. Finally, the successfully fabricated MoS<sub>2</sub>/SPCE electrode examined by electrochemical experiments.

### 3. RESULTS AND DISCUSSION

#### 3.1 Characterization of flake-like MoS<sub>2</sub>

The crystalline structure and phase composition of the as-prepared MoS<sub>2</sub> material was analyzed by XRD between 10° and 80° theta angle. Fig. 1a shows a well-defined diffraction peaks at 2θ value of 14.38, 33.63, 39.58, 44.19, 49.82, 58.38, 60.39, 68.60, 74.78 and 76.19° corresponding to (002), (101), (103), (006), (105), (110), (008), (200), (203) and (116) planes are indexed to the hexagonal structure of 2H-phase MoS<sub>2</sub> (JCPDS 37-1492) [21]. In addition, there are no additional peaks observed, indicating the high crystalline nature of MoS<sub>2</sub>. Furthermore, the crystallite grain sizes were calculated by Scherer's equation [22],

$$D = K\lambda / \beta \cos \theta \quad (1)$$

where D is average crystallite size, λ is the wavelength of X-ray radiation (0.15418 nm), k is a shape factor (0.94), θ is the diffraction angle, and β is the full width at half of the maximum (FWHM). From equation (1), the average crystalline size was found to be 16 nm.

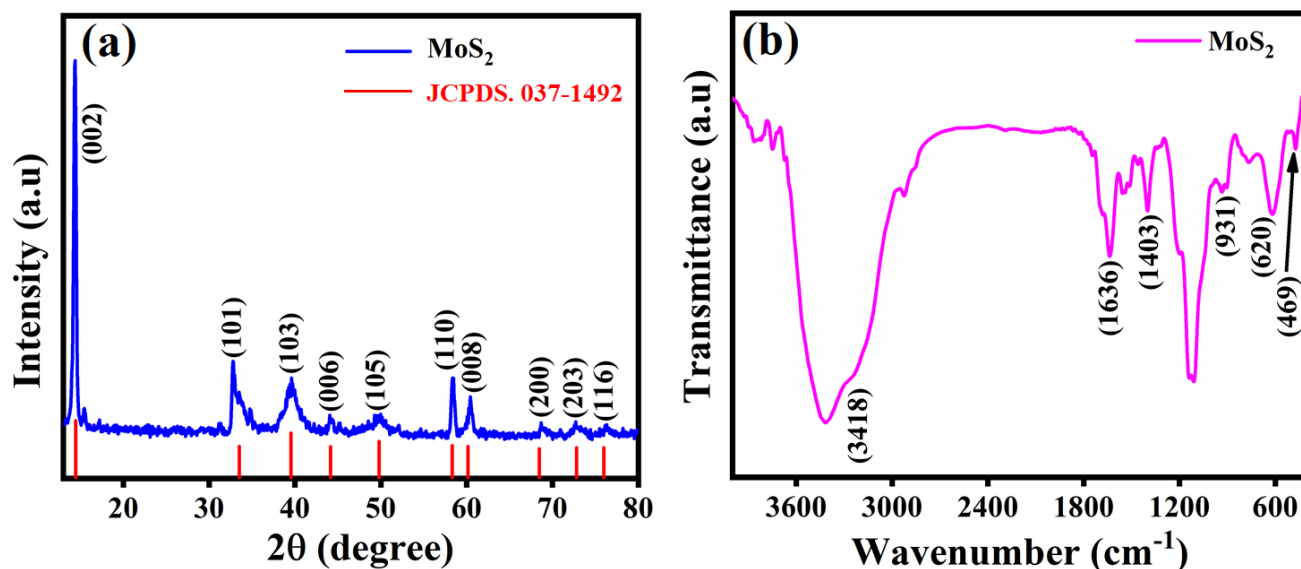


**Figure 1.** (a) XRD pattern, and (b) FT-IR spectra of the flake-like MoS<sub>2</sub>.

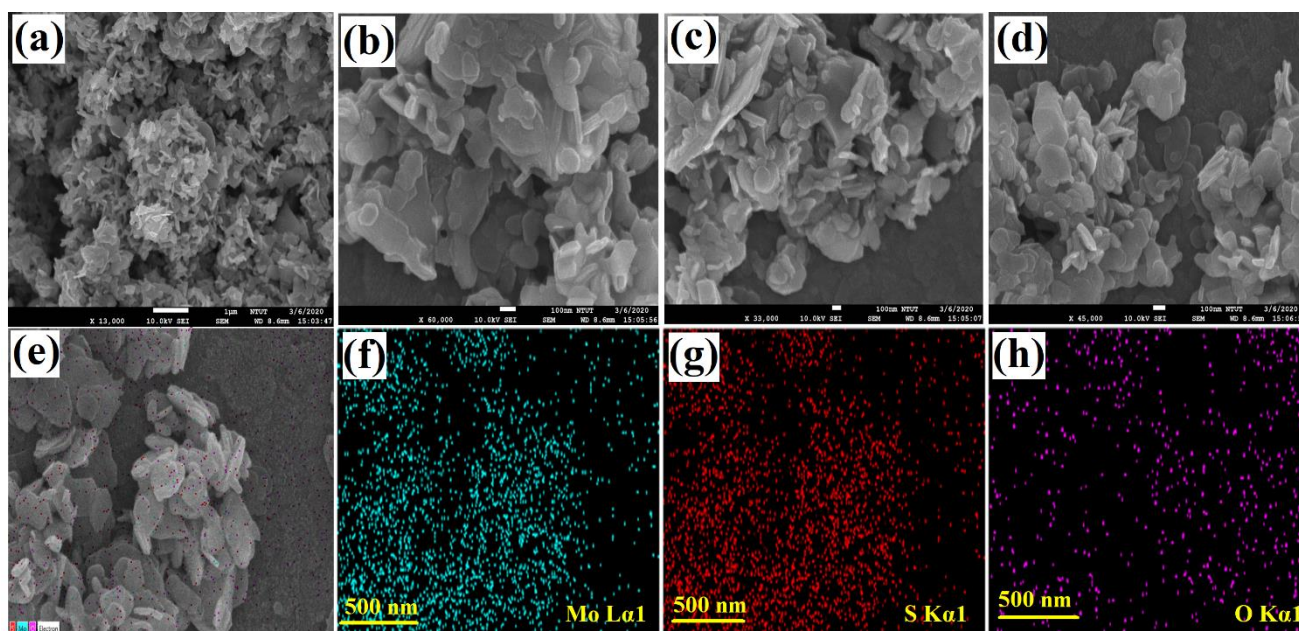


**Figure 2.** (a–d) Different magnification FE-SEM images of MoS<sub>2</sub> flake-like structure, (e) FE-SEM-elemental mapping analysis (f) Mo, (g) S, and (h) O element of MoS<sub>2</sub>.

Fig. 1b displays the FTIR spectra of flake-like MoS<sub>2</sub> were performed in the wavenumber of 4000–400 cm<sup>-1</sup>. The corresponding peak at 620 cm<sup>-1</sup> can be assigned to Mo–S-band and the peak at 1403 cm<sup>-1</sup> shows stretching vibration of S–Mo–S [22]. Moreover, the absorption peaks at 931 and 469 cm<sup>-1</sup>, which is ascribed to the S–S stretching vibration. Furthermore, the broad bands at 3418 and 1636 cm<sup>-1</sup> can be attributed to O–H or else trace amount of water molecules presented in the prepared material.

The structural and surface morphology of as-synthesized MoS<sub>2</sub> was evaluated using FE-SEM is shown in Fig. 2. From FESEM images, Fig. 2 (a–d) shows the flake-like structure with uniformly

arranged each one other. Furthermore, the flakes-like MoS<sub>2</sub> elements confirmed by EDX mapping analysis (Fig. 2 (e-h)). The observed Mo and S components are equally distributed on the surface of the material. This results demonstrated that successful formation of MoS<sub>2</sub>.

### 3.2 Electrochemical behavior of bare SPCE and flake like MoS<sub>2</sub> modified SPCE

Electrochemical impedance spectroscopy (EIS) is a very effective and explore the electrochemical behavior of modified electrodes using Randles modules circuit (inset: Fig.3a). Fig. 3a demonstrates the EIS plot of bare SPCE and MoS<sub>2</sub>/SPCE in the 0.1 M KCl solution containing 5 mM [Fe(CN)<sub>6</sub>]<sup>3-/4-</sup>. The R<sub>ct</sub> values were calculated to be 1269 Ω and 573 Ω for bare SPCE and flake-like MoS<sub>2</sub>/SPCE, respectively. The lower R<sub>ct</sub> of the modified electrode shows higher conductivity and excellent electron transfer property than that of bare SPCE. These results indicate that the prepared material is a promising catalyst in the electrochemical sensing applications.

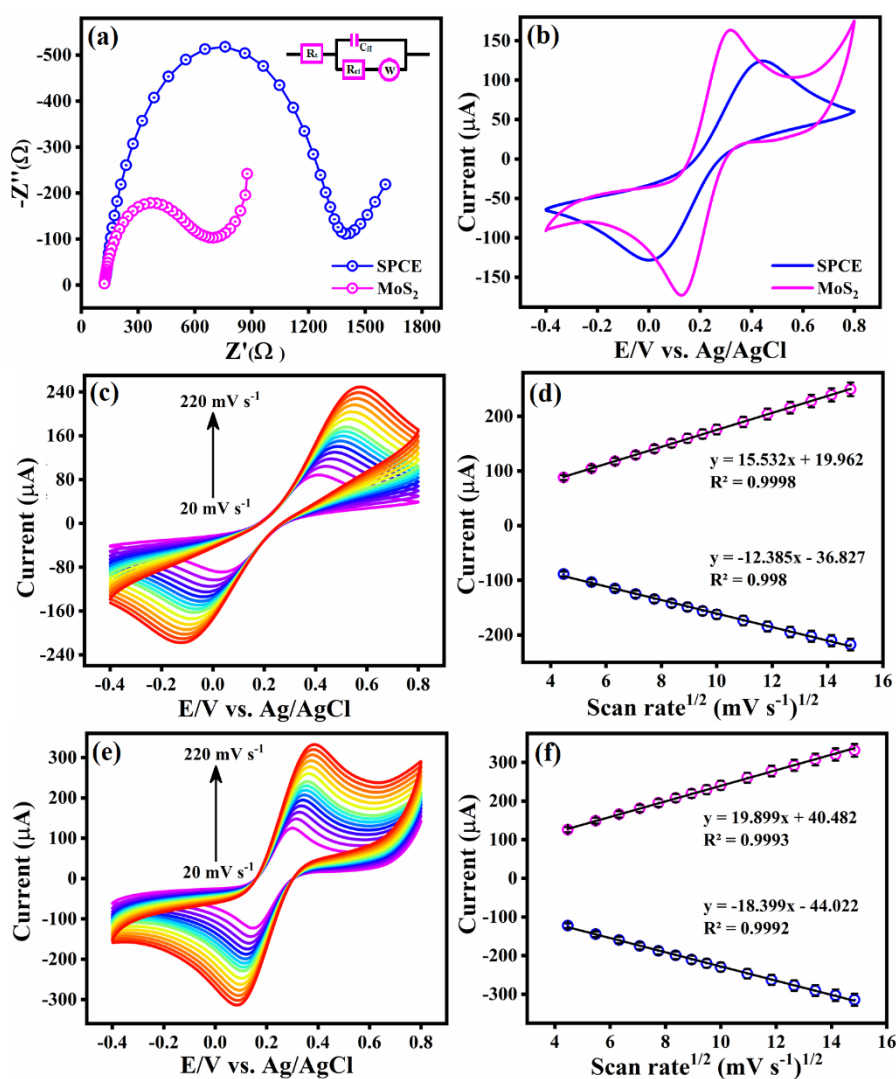


**Figure 3.** (a) EIS plot, (b) CV curve of bare SPCE and MoS<sub>2</sub>/SPCE, (c, e) The CV curve of different scan rate at 20–200 mV/s, and (d, f) corresponding calibration plot of the redox peak current and the square root of scan rate. All experiment was conducted in 5.0 mM [Fe(CN)<sub>6</sub>]<sup>3-/4-</sup>/0.1 M KCl.

The electroactive surface area was examined by CV in 5 mM ferric and ferrous cyanide solution containing 0.1 M KCl at SPCE and MoS<sub>2</sub>/SPCE at 50 mV s<sup>-1</sup> scan rate (Fig. 3b). The MoS<sub>2</sub> exhibits the oxidation and reduction peaks current is 162.6 μA, and 174.1 μA, respectively and the peak to peak separation (ΔE<sub>p</sub>) is 0.24 V. this result suggests that the fabricated electrode was higher catalytic activity than bare SPCE (*I*<sub>pa</sub> = 123.7 μA, *I*<sub>pc</sub> = 126.5 μA and ΔE<sub>p</sub> = 0.42 V). These results indicate that the proposed electrode was higher electrocatalytic activity. Fig. 3 (e, d) shows the different scan rate of the SPCE and MoS<sub>2</sub>/SPCE in the presence of 5 mM of ferrous and ferric cyanide/0.1 M KCl solution. The oxidation and reduction peaks current increased continuously with increasing the scan rate 20–200 mV/s, obtaining the overall reaction is a diffusion process. Fig. 3 (d, f) shows the linear plot of the redox peaks current and square root of the scan rate (*v*<sup>1/2</sup>). The active surface area (*A*) was measured in the following Randles –Sevcik equation (2) [23],

$$i_p = 2.69 \times 10^5 A \times D^{1/2} n^{3/2} v^{1/2} C \quad (2)$$

where *i*<sub>p</sub> is redox peak current, *D*, *n*, *v*, *C* represents diffusion coefficient, the number of electrons (e<sup>-</sup>), scan rate (mV/s) and concentration of [Fe(CN)<sub>6</sub>]<sup>3-/4-</sup> solution respectively. From equation (2), the electroactive surface area (*A*) was estimated to be 0.609 cm<sup>2</sup> and 0.78 cm<sup>2</sup> for bare SPCE and MoS<sub>2</sub>/SPCE. The higher surface area of the proposed electrode attributed to the huge performance of MT determination.

### 3.3 Electrochemical behavior of metol on the modified and unmodified electrodes

The electrochemical redox activity of metol at MoS<sub>2</sub>/SPCE and bare SPCE was carried out by CV in the absence and presence of MT containing 0.05 M PBS (pH 7) at the scan rate of 50 mV s<sup>-1</sup>.

Fig. 4a shows the bare SPCE and MoS<sub>2</sub>/SPCE in the absence of MT; there is no peak appeared in the potential window of -0.2 V to 0.4 V, and the background current of modified SPCE has very higher amounts comparing to bare SPCE. Meanwhile, the material was successfully coated on the surface of SPCE. After, the addition of 10 μM MT, a weaker pair redox peaks current were observed at bare SPCE (*I*<sub>pa</sub> = 7.31, and *I*<sub>pc</sub> = 5.01 μA), respectively. A well-defined oxidation peak current (12.69 μA) and reduction peak current (10.22 μA) were observed when adding 100 μM MT in the 0.05 M PBS (pH 7). As a result, the MoS<sub>2</sub>/SPCE displays enhanced redox couple and lower peak potential. This result demonstrated that the fabricated electrode was excellent electron transfer mediators to the determination of MT.

The effect of the loading catalyst is significant for improving current response as well as higher sensitivity on the modified electrode. Therefore, we have evaluated the various loading level is 4, 6, 8, and 10 μL (1 mg/mL) in the presence of 100 μM of MT containing 0.05 M PBS (pH 7) at 50 mV s<sup>-1</sup> scan rate are presented in Fig. 4b. It can be clearly explained that the redox response of MT gradually increases while increasing the amount of modified electrode from 4 to 8 μL. when increasing loading level above 8 μL, the current was decreased. These results suggest the high level of a modified electrode can be blocked in the electron transfer properties of the electrode and electrolyte solution. Therefore, the 8 μL of MoS<sub>2</sub> was selected for the further electrochemical sensing of MT.

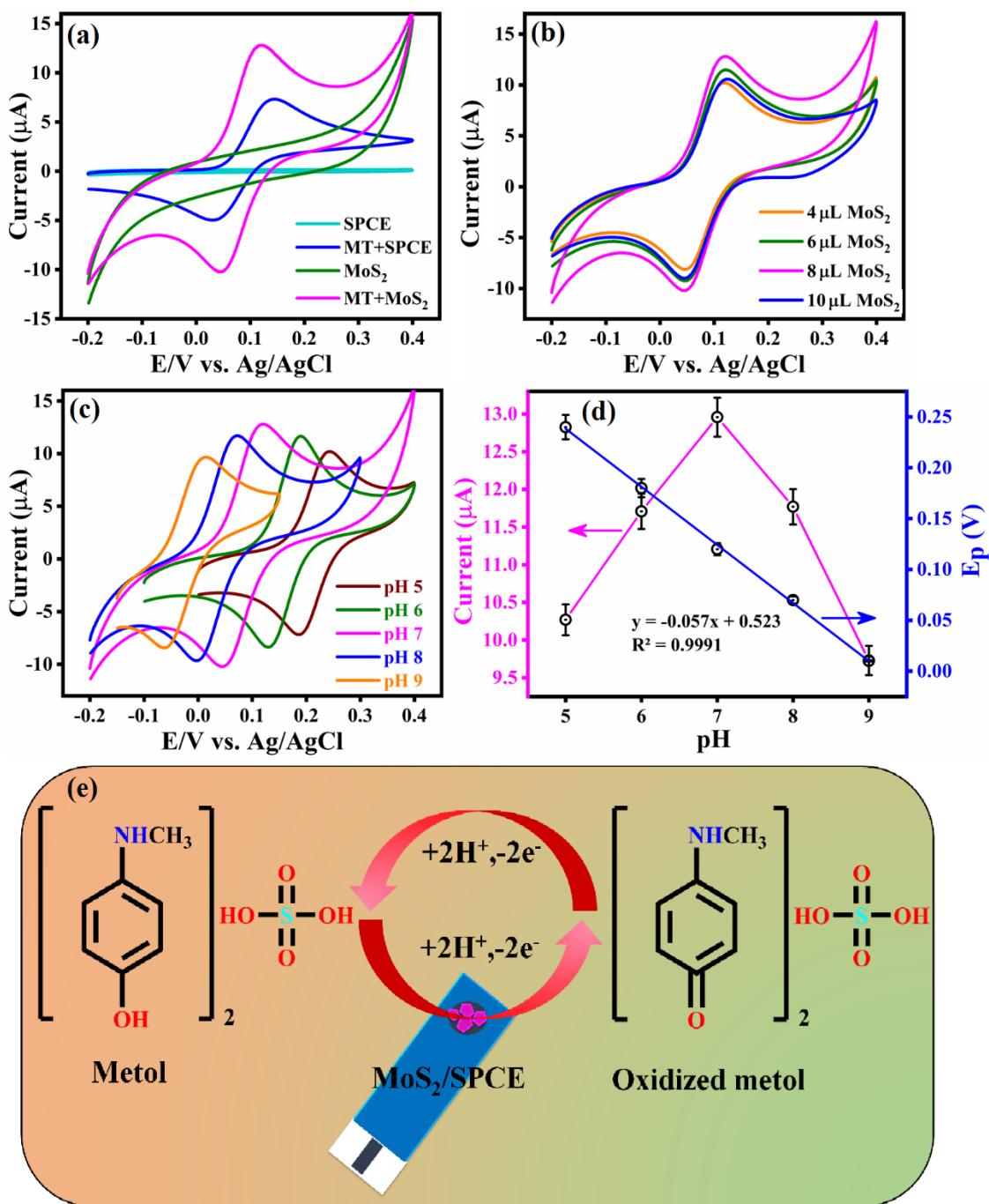


**Figure 4.** (a) CV curve of bare SPCE and MoS<sub>2</sub>/SPCE in the absence and presence of MT, (b) various loading catalysis is 4, 6, 8, and 10 μL (mg/mL), (c) CV response of different pH from 5 to 9 (0.05 PBS). (d) the linear plot between oxidation peak current and peak potential versus different pH. All the experiment were performed, N<sub>2</sub>-saturated 0.05 M PBS (pH 7) in 00 μM MT, and (e) the possible electrochemical redox mechanism of MT.

### 3.4 Effect of pH

The effect of pH is beneficial to interact the proton to electron participated in the electrolyte solution to investigate the redox property of 100 μM MT was performed by CV in 0.05 M PBS with

various pH at 50 mV s<sup>-1</sup> scan rate. From Fig. 4c, it was observed that the redox potential shifted to a negative direction when increasing the pH values from 5 to 7, then increasing pH from 7 to 9 with decreasing redox peak current. This result is indicating pH 7 was higher peak current obtained. Therefore, pH 7 was using further electrochemical studies, as shown in Fig. 4d (blue line). As shown in Fig. 4d (black line) display the corresponding linear plot of the various pHs and the redox peak potential. The linear regression equation is  $E_{pa} \text{ (V)} = -0.057 C [\text{pH}] - 0.523$  ( $R^2 = 0.9991$ ). The obtained slop value (-0.057 V) is close to the Nernstian slope value [24]. Above the results conclude that the equal number of electrons and protons participated. The possible redox mechanism of 4-(methylamino) phenol sulfate to 4-(methylamino)-1λ<sup>5</sup>- benzenone sulfate (oxidized metol) as shown in Fig. 4e [25].

### 3.5 Effect of concentration

The electrocatalytic performance was further confirmed by CV with different concentrations of MT from 0 to 400 μM at 50 mV s<sup>-1</sup> scan rate in 0.05 M PBS (pH 7) as shown in Fig. 5a. The redox peaks current of MT was increasing linearly when increasing the various addition of MT from 0 to 400 μM as shown in Fig.5b, the linear plot of the redox current peak and the concentration of MT. The linear regression as  $I_{pa} \text{ (}\mu\text{A)} = 0.0877 C \text{ (}\mu\text{M)} + 4.6129$  ( $R^2 = 0.9835$ ) and  $I_{pc} \text{ (}\mu\text{A)} = 0.0639 C \text{ (}\mu\text{M)} - 3.823$  ( $R^2 = 0.9881$ ). Furthermore, the calibration plot between the *logarithm* of redox peak current and *logarithm* of concentration as shown in Fig. 5c. The corresponding regression equation with coefficient as  $I_{pa} \text{ (}\mu\text{A)} = 0.7955 C \text{ (log MT)} - 0.4735$  ( $R^2 = 0.996$ ) and  $I_{pc} \text{ (}\mu\text{A)} = 0.7706 C \text{ (log MT)} - 0.5404$  ( $R^2 = 0.9982$ ), respectively. This results suggesting the fabricated sensor has first-order kinetics during the sensing of MT. These results show the excellent catalytic activity of MoS<sub>2</sub> modified electrode towards metol detection.

### 3.6 Effect of scan rate

The effect of scan rate was examined by CV by MoS<sub>2</sub>/GCE in 100 μM MT with different scan rates from 20–200 mV s<sup>-1</sup> in 0.05 M PBS (pH 7) are displayed in Fig. 5d. The redox peak current increases linearly with increasing scan rate range from 20 to 200 mV s<sup>-1</sup>. Fig. 5e shows the linear plot of the redox peak current and square root of the scan rate. The linear regression equation as  $I_{pa} \text{ (}\mu\text{A)} = 1.2489 C \text{ (mV s}^{-1}\text{)} + 0.7675$  ( $R^2 = 0.9986$ ) and  $I_{pc} \text{ (}\mu\text{A)} = -1.0461 C \text{ (mV s}^{-1}\text{)} - 0.7321$  ( $R^2 = 0.9986$ ). As results indicate that the overall kinetics should be diffusion-controlled process on MoS<sub>2</sub> modified SPCE. Fig. 5f shows the linear plot of the *logarithm* of peak current and *logarithm* of the scan rate with linear regression is  $\log I_p \text{ (}\mu\text{A)} = 0.4559 C \text{ (mV s}^{-1}\text{)} + 0.2084$  ( $R^2 = 0.997$ ). The obtained slope value is 0.455, very close to the theoretical value of 0.5 [26]. Based on these results demonstrates that the electrochemical redox process is the purely diffusion-controlled process [27].

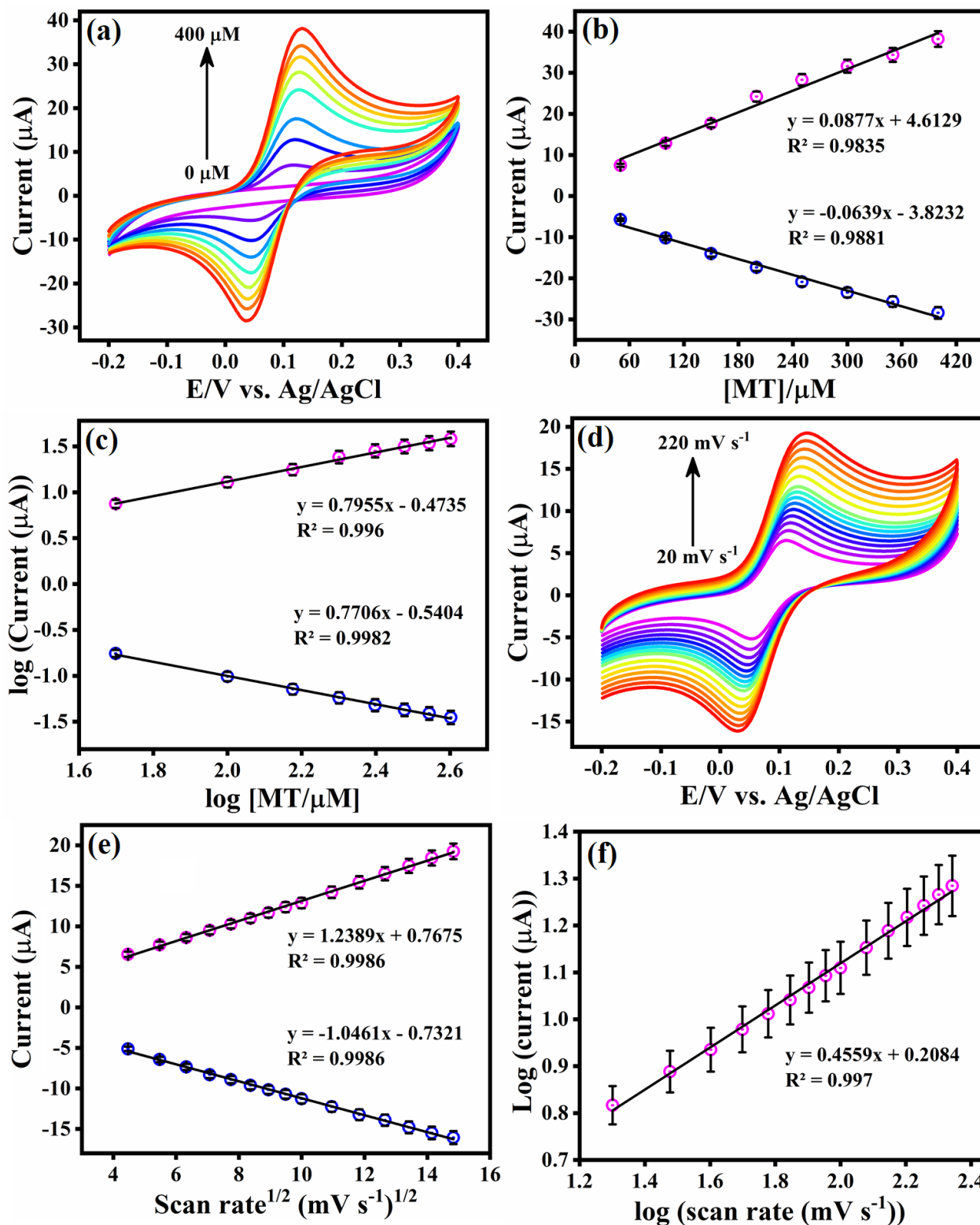


**Figure 5.** (a) CV profile of MoS<sub>2</sub>/SPCE in 0.05 M PBS (pH 7) containing different addition of MT range from 0 to 400 μM, (b) The linear plot between redox peak current and different addition of MT (μM), (c) the corresponding linear plot of the *logarithm* redox peak current and the *logarithm* MT concentration, (d) CV curve of MoS<sub>2</sub>/SPCE in the 100 μM MT at different scan rate range from 20 to 220 mV s<sup>-1</sup>. (e) The calibration plot of redox peak current versus scan rate, and (f) The redox peak potential ((E<sub>pa</sub> + E<sub>pc</sub>)/2) versus the *logarithm* of the scan rate. All experiments were carried out in N<sub>2</sub>-saturated 0.05 M PBS (pH 7).

## 3.7 Differential pulse voltammetry of metal

DPV is a highly sensitive, excellent resolution and better selectivity when compare to other voltammetric. Hence, we have selected the DPV technique to determine the lower concentration of MT on MoS<sub>2</sub> modified SPCE in containing 0.05 M PBS (pH 7) are presented in Fig. 6a. The oxidation peak current increases linearly while adding low to high concentration of MT from 0.2  $\mu$ M to 1211  $\mu$ M.

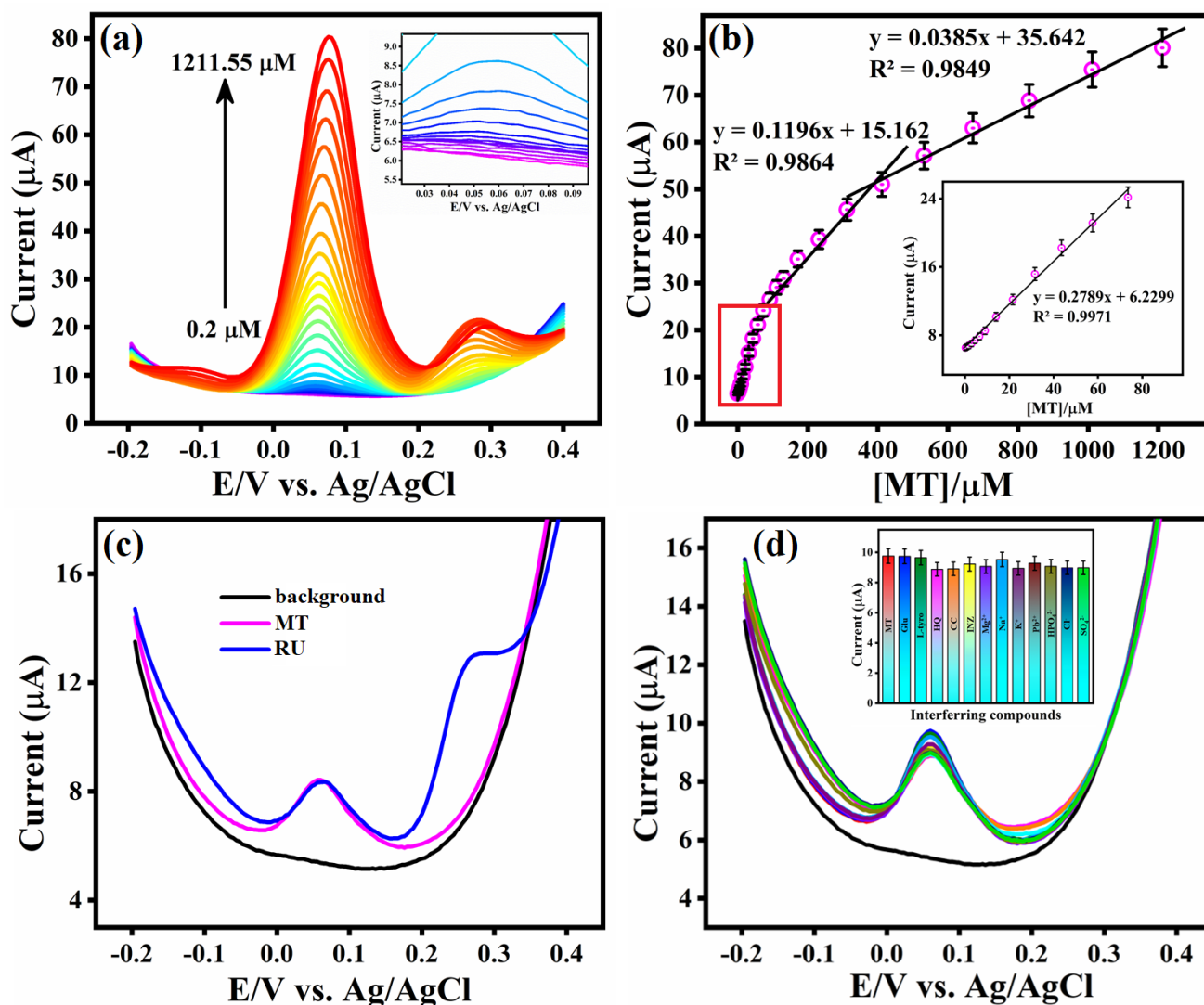


**Figure 6.** (a) DPV curve of MoS<sub>2</sub>/SPCE with different concentration of MT range from 0.2 to 1211.55  $\mu$ M in N<sub>2</sub>-saturated 0.05 M PBS (pH 7) (inset: low concentration of MT), (b) the corresponding linear plot between oxidation peak current and various addition MT (inset: first linear range), (c) selectivity of simultaneous detection of MT and RU, and (d) The selectivity variable co-interfering species: Glu, L-tyro, HQ, CC, INZ; Mg<sup>2+</sup>, Na<sup>+</sup>, K<sup>+</sup>, Pd<sup>2+</sup>, HPO<sub>4</sub><sup>2-</sup>, Cl<sup>-</sup>, and SO<sub>4</sub><sup>2-</sup> (inset: oxidation peak current of interfering compounds).

As shown in Fig. 6b, the calibration linear plot of oxidation peak current versus the different concentration of MT. Three linear range were obtained. The first linear range from 0.2 to 71  $\mu$ M, the observed the linear calibration equation as  $I_{pa}$  ( $\mu$ A) = 0.2789 C ( $\mu$ M) + 6.2299 ( $R^2 = 0.9971$ ). the

calculated analytical parameters from first linear range, the calculated limit of detection 0.01  $\mu\text{M}$  with sensitivity of  $1.05 \mu\text{A } \mu\text{M}^{-1} \text{cm}^{-2}$  and LOD calculate from the following equation,<sup>22</sup>

$$LOD = 3\sigma/S \quad (3)$$

where S indicates the slope value of linear plot and  $\sigma$  is represents the relative standard deviation (RSD). The obtained analytical parameters including a wide linear range, good sensitivity with a lower detection limit of MT on  $\text{MoS}_2/\text{SPCE}$  was compared with previously reported sensors [25, 27, 30–33] are summarized in Table 1. From the table 1, the LOD on our fabricated flake-like sensor was lower detection than that of other modified electrode such as  $\text{LiCoO}_2$  [33], Au NPs [34], CTS- $\text{TiO}_2$  [25], IL [35], and MWNT [36] as presented in Table 1.

Generally,  $\text{MoS}_2$  has great attention in recent years. Because of their unique optical [28], and physical-electrochemical properties, and also the potential application of larger surface area, better chemical stability [29], equal particle size distribution [30] and high porosity [31] compare with  $\text{ZrO}_2(20\%)/\text{Nano-ZSM-5}$  [32] and  $\text{CaSnO}_3$  [25]. Therefore, we have synthesized flakes like  $\text{MoS}_2$  demonstrates a wide range of potential and excellent catalytic performance towards electrochemical detection of MT.

**Table 1.** Comparison of flake-like  $\text{MoS}_2$  modified electrode with various sensors in metal detection

Modified electrode	method	linear range ( $\mu\text{M}$ )	detection limit ( $\mu\text{M}$ )	ref
$\text{CaSnO}_3/\text{GCE}$	DPV	0.01–157	0.003	25
CTS <sup>a</sup> - $\text{TiO}_2/\text{CILE}^b$	DPV	0.08–800	0.0237	27
$\text{ZrO}_2(20\%)/\text{Nano-ZSM-5}^c/\text{GCE}$	DPV	0.004–800	0.001	32
$\text{LiCoO}_2/\text{CILE}^b$	DPV	0.4–400	0.246	33
Au NPs/ $\text{CMWE}^d$	DPV	2–800	0.64	34
IL <sup>e</sup> / $\text{CPE}^f$	DPV	5–1000	2.33	35
MWNT <sup>g</sup> / $\text{GCE}$	CV	$10 \mu\text{M}–8 \times 10^{-2} \text{M}$	5	36
$\text{MoS}_2/\text{SPCE}$	DPV	0.2–1211	0.01	This work

<sup>a</sup>chitosan, <sup>b</sup>carbon ionic liquid electrode, <sup>c</sup>nanocrystalline ZSM-5 zeolite, <sup>d</sup>carbon molecular wire electrode, <sup>e</sup>ionic liquid, <sup>f</sup>carbon paste electrode, <sup>g</sup>multiwall carbon nanotubes.

### 3.8 Simultaneous selectivity of the sensor

The effect of variable potentially anti-interference study were performed by DPV in 0.05 PBS (pH 7) containing 20  $\mu\text{M}$  MT at  $\text{MoS}_2/\text{SPCE}$ . As shown in Fig. 6c, the selectivity of simultaneous detection of MT and Rutin (RU–200  $\mu\text{M}$ ), which shows the oxidation peak potential of 0.26 V (RU) respectively. The 20-fold higher concentration of RU has does not affect the original oxidation peak current and peak potential of original MT. In addition, the proposed sensor for the determination of MT in the presence of various biological compounds (10-fold concentration) such as glucose (Glu), L-tyrosine (L-tyro), hydroquinone (HQ), catechol (CC), and isoniazid (INZ) and some common metal ions

including  $\text{Mg}^{2+}$ ,  $\text{Na}^+$ ,  $\text{K}^+$ ,  $\text{Pd}^{2+}$ ,  $\text{HPO}_4^{2-}$ ,  $\text{Cl}^-$ , and  $\text{SO}_4^{2-}$  (Fig. 6d, inset: bar diagram of peak current). From the DPV current response, there is significantly decreased current values, the RSD value is less than 3% in from original current response. These results demonstrating that higher selectivity of as prepared modified electrode towards the detection of MT.

### 3.9 Stability, reproducibility, and repeatability

The stability of the constructed sensor was carried out by CV with 100 continuous cycles (Fig. 7a) in 0.05 M PBS, (pH 7) in 100  $\mu\text{M}$  MT at sweeping scan rate 50 mV/s. The obtained oxidation peak current loosed only less than 3.5% during the 100 cycles. This results suggesting that the  $\text{MoS}_2$  shows good stability, due to some structural and chemical properties.

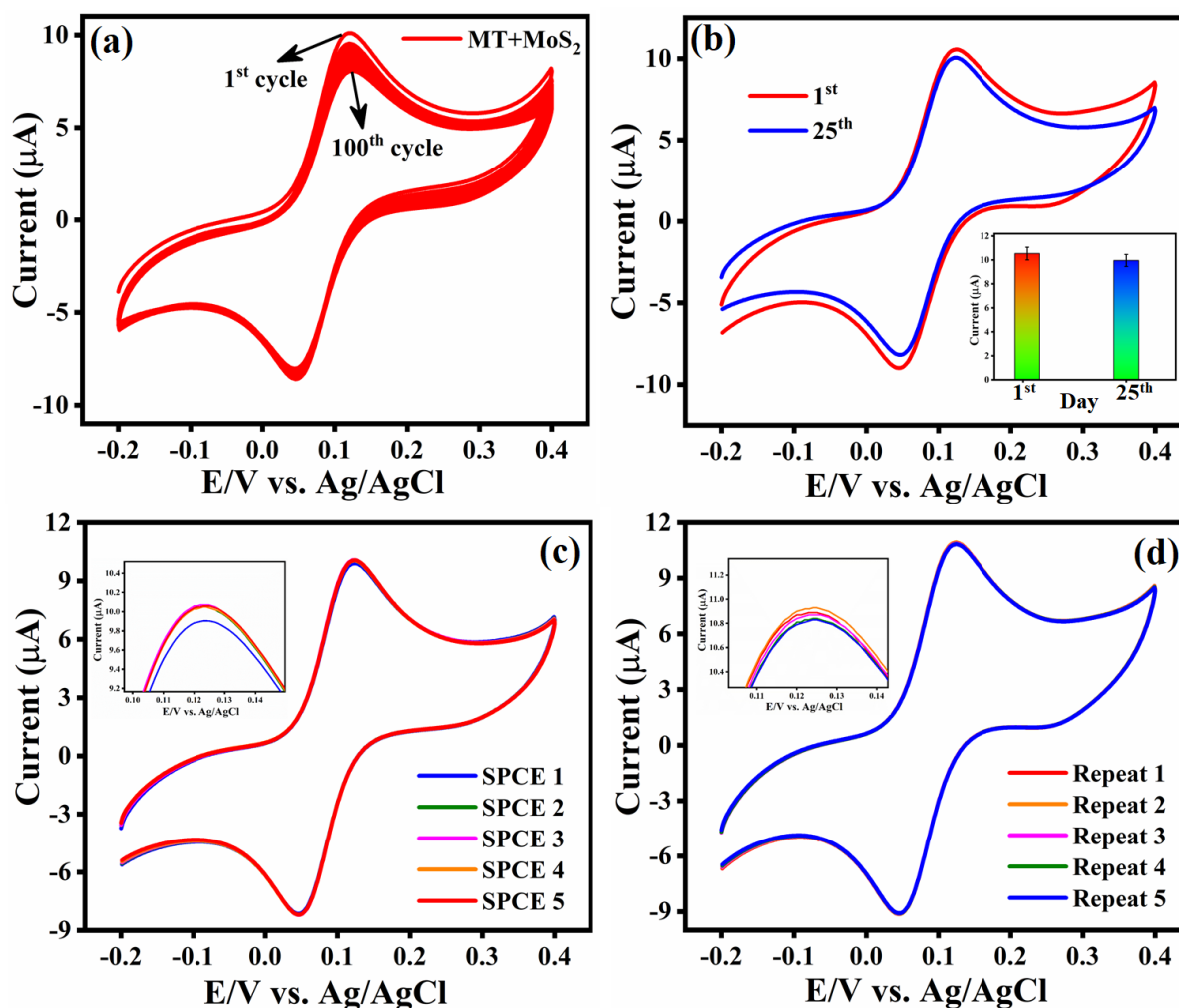


**Figure 7.** (a) CV curve of cyclic stability of 100 cycles in the  $\text{MoS}_2/\text{SPCE}$ , (b) storage stability (the result of bar diagram), (c) reproducibility of five independent electrodes, and (d) repeatability. All measurements were carried out by CV with  $\text{N}_2$ -saturated containing 0.05 M PBS (pH 7) containing 100  $\mu\text{M}$  MT at 50  $\text{mV s}^{-1}$  scan rate.

In addition, the storage stability was investigated by the CV in  $N_2$  saturated 0.05 M PBS (pH 7) containing 100  $\mu\text{M}$  MT at the sweeping scan rate of  $50 \text{ mV s}^{-1}$  under the optimal conditions (Fig. 7b). The modified electrode current response exhibits about 95.6%, which reveals that the excellent long term stability as well as electrocatalytic redox property of MT.

The reproducibility of  $\text{MoS}_2/\text{SPCE}$  was performed by the various electrode for 5 independent experiments (Fig. 7c) in 100  $\mu\text{M}$  MT containing 0.05 M PBS (pH 7) and obtained RSD is 3.32%, indicating that the fabricated sensor has highly reproducible. Moreover, the fabricated electrodes were successfully examined by CV in the evaluation of repeatability for the MT sensor (Fig. 7d). The oxidation peak current displayed in the crucial current difference with the RSD value of 2.96% for 100  $\mu\text{M}$  MT in 0.05 M PBS (pH 7). It may conclude that the  $\text{MoS}_2/\text{SPCE}$  had superior repeatability of the sensor.

### 3.10 Real sample analysis

The flake-like  $\text{MoS}_2$  modified electrode was successfully applied for various water real samples such as a river and tap water (Fig. 8). The prepared samples were collected from Taiwan. Further, the prepared known concentration of MT was spiked in the unknown concentration of real samples. The recovery results is measured using the relative standard deviation method are displayed in Table 2. Based on these results, the recoveries values of river water and tap water samples are found to be 97.6% to 99.2% and 96.0% to 99.6% the average RSD value of 2.4% and 1.9%, indicating the practical applications of  $\text{MoS}_2$  modified electrode for the metal detection in water real samples with good recoveries.

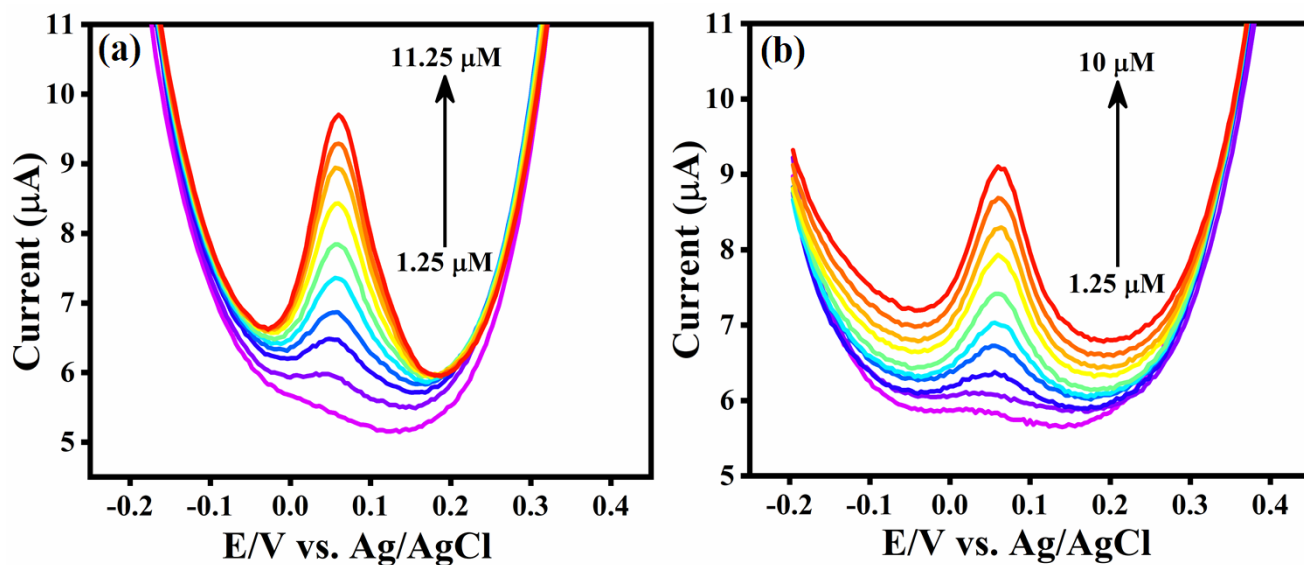


**Figure 8.** DPV response of real sample (a) river water and (b) tap water in 0.05 M PBS (pH 7) with various amount of MT.

**Table 2.** Results for the determination of MT in water real samples

Sample	Spiked ( $\mu\text{M}$ )	Found ( $\mu\text{M}$ )	RSD (%)	Recovery (%)
River water	1.25	1.22	3.2	97.6
	2.50	2.47	2.4	98.8
	3.75	3.72	2.0	99.2
	5.00	4.98	1.9	99.6
	6.25	6.24	1.4	99.8
	7.50	7.48	0.8	99.7
	8.75	8.74	0.9	99.8
	10.00	9.97	1.1	99.7
	11.25	11.24	1.0	99.9
Tap water	1.25	1.23	3.1	96.0
	2.50	2.41	2.7	96.4
	3.75	3.67	2.4	97.8
	5.00	4.90	2.0	98.0
	6.25	6.21	1.8	99.2
	7.50	7.47	1.1	99.6
	8.75	8.68	1.3	99.2
	9.50	9.47	1.5	99.6
	10.00	9.94	0.9	99.4

#### 4. CONCLUSION

In this work we have successfully prepared by flake-like  $\text{MoS}_2$  material through hydrothermal method for electrochemical detection of metol. The morphology and crystalline structure of as-synthesised materials were confirmed by several analytical spectroscopy characterizations such as XRD, FTIR, FESEM, EDX-elemental mapping. The electrochemical activity of modified SPCE performed as an efficient electrocatalyst to enhance the electrocatalytic response of MT and demonstrates a lower detection limit is  $0.01 \mu\text{M}$ , and a wide linear range from  $0.2$  to  $1211 \mu\text{M}$  with a better sensitivity. Moreover, the proposed electrode shows superior selectivity, stability, reproducibility, and repeatability. For real samples analysis, the sensor displays excellent recoveries on  $\text{MoS}_2/\text{SPCE}$  towards electrochemical detection of MT in water real samples with satisfactory results.

#### ACKNOWLEDGMENTS

The authors are grateful for the financial support ((MOST 106-2113-M-027-003-MY3 to S.M.C) from the Ministry of Science and Technology (MOST), Taiwan.

#### ORCID

Shen-Ming Chen: 0000-0002-8605-643X

Arumugam Sangili: 0000-0001-9628-0067

## References

1. L. S. Samanta and R. Srivastava, *J. Electroanal. Chem.*, 777 (2016) 48–57.
2. B.M. Praveen and T.V. Venkatesha, *Int. J. Electrochem. Sci.*, 4 (2009) 2414–275.
3. R. R. Krishna and C. S. P. Sastry, *Fresenius J. Anal. Chem.*, 296 (1979) 46.
4. L. Lunar, D. Sicilia, S. Rubio, D. P. Rez-Bendito and U. Nickel, *Wat. Res.*, 34 (2000) 1791–1802.
5. J. Liao and P. Wang, *Anal. Chem. photog. Chemi.* Chinese Film Press, Beijing, (1981).
6. R. Androzzzi, V. Caprio, A. Insola, and R. Marotta, *Wat. Res.*, 34 (2000) 463–472.
7. L. Lunar, D. Sicilia, S. Rubio, D. P. Rez-Bendito and U. Nickel, *Wat. Res.*, 34 (2000) 3400–3412.
8. Z. R. Meng, R. Zhao and X. R. Liu, *Fenxi Kexue Xuebao*, 16 (2000) 314.
9. Q. Li, N. Zhang, Y. Yang, G. Wang and D. H. L. Ng, *Langmuir*, 30 (2014) 8965–8972.
10. X. Zhou, B. Xu, Z. Lin, D. Shu and L. Ma, *J. Nanosci. Nanotechnol.*, 14 (2014) 7250.
11. H. Hwang, H. Kim and J. Cho, *Nano Lett.*, 11 (2011) 4826–4830.
12. M. B. Askari, A. Beheshti-Marnani, M. Seifi, S. M. Rozati and P. Salarizadeh, *J. Collo. Inter. Sci.*, 537 (2019) 186–196.
13. K. Nguyen-Ba, J. R. Vargas-García and A. Manzo-Robledo, *Mat. Sci. Eng. B-Adv.*, 256 (2020) 114539.
14. B. Mohanty, M. Ghorbani-Asl, S. Kretschmer, A. Ghosh, P. Guha, S. K. Panda, B. Jena, A. V. Krashennnikov and B. K. Jena, *ACS Catal.*, 8 (2018) 1683–1689.
15. R. Sakthivel, S. Dhanalakshmi, S.-M. Chen, T.-W. Chen, V. Selvam, S. K. Ramaraj, W.-H. Weng and W.-H. Leung, *Int. J. Electrochem. Sci.*, 12 (2017) 9288–9300.
16. R. Sha, N. Vishnu and S. Badhulika, *Sensor Actuat. B-Chem.* 279 (2019) 53–60.
17. L.-C. Wang, S.-K. Bao, J. Luo, Y.-H. Wang, Y.-C. Nie and J.-P. Zou, *Int J Hydro. Ene.*, 41 (2016) 10737–10743.
18. H. R. Inta, T. Biswas, S. Ghosh, R. Kumar, S. K. Jana and V. Mahalingam, *Chem. Nano Mat.*, 6 (2020) 685–695.
19. A. Zak, Y. Feldman, V. Alperovich, R. Rosentsveig and R. Tenne, *J. Am. Chem. Soc.*, 122 (2000) 11108–11116.
20. R. Kumar, N. Goel and M. Kumar, *Appl Phys Lett.*, 112 (2018) 053502.
21. P. R. Kumar, Y. H. Jung and D. K. Kim, *RSC. Adv.*, 5 (2015) 79845–79851.
22. K. C. Lalithambika, K. Shanmugapriya and S. Sriram, *Appl. Phys. A-Mater.*, 125 (2019) 817.
23. V. Vinothkumar, A. Sangili, S.-M. Chen, P. Veerakumar and K.-C. Lin, *New J. Chem.*, 44 (2020) 2821.
24. V. Vinothkumar, A. Sangili, S.-M. Chen, T.-W. Chen, M. Abinaya and V. Sethupathi, *Int. J. Electrochem. Sci.*, 15 (2020) 2414–2429.
25. B. Muthukutty, A. Krishnapandi, S.-M. Chen, M. Abinaya and A. Elangovan, *ACS Sustain. Chem. Eng.*, 8 11 (2020) 4419–4430.
26. A. Sangili, M. Annalakshmi, S.-M. Chen, P. Balasubramanian and M. Sundrarajan *Compos. B. Eng.*, 162 (2019) 33–42.
27. X. Niu, L. Yan, X. Li, A. Hu, C. Zheng, Y. Zhang and Wei Sun, *Int. J. Electrochem. Sci.*, 11 (2016) 1720–1729.
28. J. Li, C. L. Hu, H. Wu, Z. X. Liu, S. Cheng, W. F. Zhang, H. B. Shu and H. X. Chang, *Cryst. Growth Des.*, 16 (2016) 7094–7101.
29. Y. Zhang, P. Chen, F. Wen, B. Yuan and H. Wang, *J. Electroanal. Chem.*, 761 (2016) 14–20.
30. Y. Chen, B. Song, X. Tang, L. Lu and J. Xue, *small*, 10 (2014) 1536–1543.
31. Z. Cheng, B. He and L. Zhou, *New J. Chem. A*, 3 (2015) 1042.
32. B. Kaur, B. Satpati and R. Srivastava, *RSC Adv.*, 6 (2016) 65736.
33. W. Sun, Y. Deng, J. Liu, W. Liu, Y. Cheng, L. Wang and Y. Gu, *Thin Solid Films*, 564 (2014) 379–383.
34. X. Niu, L. Yan, Z. Wen, X. Li, Y. Niu, Y. Lu and W. Sun, *Anal. Lett.*, 50 (2017) 325–335.

35. W. Sun, Q. Jiang and K. Jiao, *J. Solid State Electrochem.*, 13 (2009) 1193–1199.  
35. J. Li, Y. Wang, and Z. Liu, *Russ. J. Electrochem.*, 42 (2006) 27–30.

© 2020 The Authors. Published by ESG ([www.electrochemsci.org](http://www.electrochemsci.org)). This article is an open access article distributed under the terms and conditions of the Creative Commons Attribution license (<http://creativecommons.org/licenses/by/4.0/>).